symmetry

MDPI

Article

The Missing Relationship between the Miscibility of Chiral Dopants and the Microscopic Dynamics of Solvent Liquid Crystals: A Molecular Dynamics Study

Go Watanabe [1,2,*,†], Akane Yamazaki [1] and Jun Yoshida [3,*]

[1] School of Science, Kitasato University, Sagamihara 252-0373, Japan
[2] Kanagawa Institute of Industrial Science and Technology, Kawasaki 243-0435, Japan
[3] Graduate School of Integrated Basic Sciences, Nihon University, Tokyo 156-8550, Japan
* Correspondence: go0325@kitasato-u.ac.jp (G.W.); yoshida.jun@nihon-u.ac.jp (J.Y.)
† Current address: School of Frontier Engineering, Kitasato University, Sagamihara 252-0373, Japan.

Abstract: Nematic liquid crystals (LCs) are known to undergo a phase transition to chiral nematic LCs possessing helices upon doping with enantiomeric molecules known as chiral dopants. The relationship between the helical pitch (p), the molar fraction (x), and the power of the chiral dopant to induce a helix in a nematic solvent (β_M) is expressed as $p = 1/(x \cdot \beta_M)$. The helical pitch is easily controlled by the concentration of the chiral dopant when the dopant molecule is miscible with the host nematic LC. However, it has not yet been clarified what the miscibility of the chiral dopant molecules with the nematic LCs depends. Therefore, we performed all-atom molecular dynamics (MD) simulations for the system composed of both Δ and Λ isomers of a chiral dopant molecule dispersed in a nematic LC and investigated the relationship between the microdynamics of the chiral molecules and their miscibility with the nematic solvent. The miscibility of the chiral dopant molecules with the LC solvent was found to correlate with the diffusion coefficient of the LC solvent. In the system where the chiral dopant molecules with high miscibility were added, the diffusion coefficient of the LC solvents was comparable to that of the system in which the chiral molecule was not doped. Furthermore, it was confirmed that more elongated chiral dopants were more miscible with the nematic solvent consisting of calamitic molecules, and that these dopant molecules did not have a significant effect on the diffusion behavior of the LC molecules.

Keywords: chiral nematic liquid crystals; molecular dynamics simulation; miscibility; diffusion coefficient

Citation: Watanabe, G.; Yamazaki, A.; Yoshida, J. The Missing Relationship between the Miscibility of Chiral Dopants and the Microscopic Dynamics of Solvent Liquid Crystals: A Molecular Dynamics Study. *Symmetry* **2023**, *15*, 1092. https://doi.org/10.3390/sym15051092

Academic Editor: Cosimo Cardellicchio

Received: 17 March 2023
Revised: 6 May 2023
Accepted: 11 May 2023
Published: 16 May 2023

1. Introduction

It is generally well known that a nematic liquid crystal (LC) undergoes a phase transition to a chiral nematic LC possessing a helix when doped with enantiomeric molecules known as chiral dopants [1–4]. The chiral nematic LC exhibits selective reflection of circularly polarized light corresponding to the helical pitch. The pitch of the induced helicoidal superstructure is usually within the visible wavelength range. As the helical pitch can be tuned by the type and concentration of the chiral dopants, chiral nematic LCs have the potential to be utilized for photonic applications in areas of tunable mirrorless lasing [5–7], reflective colored displays [8–10], energy-saving smart windows [11–13], and sensors [14,15].

The relationship between the helical pitch (p), the molar fraction (x), and the power of the chiral dopant used to induce a helix in a nematic solvent (helical twisting power, denoted as β_M) is expressed as follows: $p = 1/(x \cdot \beta_M)$. The sign of the β_M value indicates the helical direction, where positive and negative values correspond to *P*- and *M*-helical structures, respectively.

The rational prediction of β_M of the chiral dopant is associated with the precise control of the helical structure of chiral nematic LCs. Although the helix formation in chiral nematic LCs is well understood as a macroscopic physical phenomenon, predicting the values of β_M rationally remains a challenging task based on the dopant and LC molecules. Slight differences of the molecular structure of the dopant may sometimes lead to large differences in the value of β_M.

Unlike predicting the values of β_M of the chiral dopant, the helical pitch is easily controlled by the concentration of the chiral dopant when the dopant molecule is miscible with the host nematics. However, the key factor determining the miscibility of chiral dopant molecules with nematic LCs has not yet been clarified.

The molecular shape of the chiral dopant may be one possible factor affecting its miscibility with nematics. To clarify the relationship between the molecular shape and miscibility of the chiral dopant molecule, octahedral ruthenium complexes, especially [Ru(acac)$_3$] (acac = acetylacetonate ion), are suitable chiral dopants; they have rigid and C_3 symmetric central cores, and their shapes can be systematically changed by the introduction of elongated moieties to one of the acac ligands. In previous studies, the helical twisting powers of ruthenium complex dopants were investigated using elongated ligands (**Ru-trop**) [16] and simple bromo groups (**Ru-Br0** and **Ru-Br1**) for comparison [17] (Figure 1). **Ru-Br0** and **Ru-Br1** are miscible with *N*-(4-methoxybenzylidene)-4-butylaniline (MBBA), which is well-known to show a nematic LC phase at room temperature, at no more than 0.2 mol%, while no precipitation of the dopant was observed using polarized optical microscopy for ~4.0 mol% of **Ru-trop** in MBBA [16]. There was no significant difference in the viscosity among these chiral LC mixtures with low concentrations of the chiral dopants. The difference in the microscopic behavior of these ruthenium complexes may be the cause of the difference in miscibility, but it is challenging to confirm this experimentally.

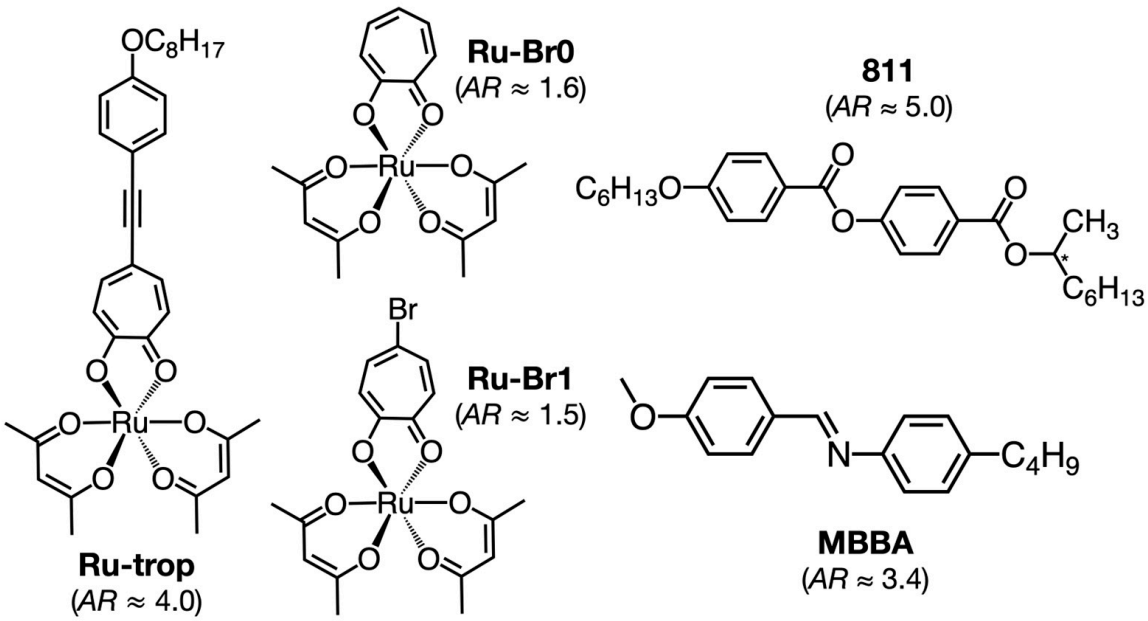

Figure 1. Molecular structures of Δ-isomers of ruthenium complexes (**Ru-trop**, **Ru-Br0**, and **Ru-Br1**) and an organic compound (**811**) used as a chiral dopant and the nematic LC (MBBA) used as a host. The values in the brackets for the ruthenium complexes and organic compounds represent the aspect ratio of the molecular length parallel to the C_2 axis to that perpendicular to the C_2 axis and that of the molecular long axis to the short axis, respectively.

We herein present new insights into the dynamics of chiral dopants at the atomic level, which are related to their macroscopic miscibility with nematic solvents. To achieve this, we conducted all-atom molecular dynamics (MD) simulations.

2. Models and Methods

In this study, all-atom MD simulations were performed using the program GROMACS 2016.3. The simulated racemic system consisted of both Δ- and Λ-enantiomers of a chiral dopant molecule dispersed in the nematic LC molecules, as previously proposed. This approach was taken because it is currently not realistic to perform all-atom MD simulations for chiral nematic LC systems exhibiting a helical structure with a sub-micrometer pitch [18]. While this approach cannot reproduce the macroscopic helical structure, it is sufficient for investigating the microscopic behavior of the LC molecules and the dopants. Three types of chiral ruthenium complex compounds, **Ru-Br0**, **Ru-Br1**, and **Ru-trop**, with different solubilities in the nematic solvents, and one chiral organic compound, **811**, with high miscibility in the nematics, as shown in Figure 1 were selected as the chiral dopants. The **811** compound has a mesogen core, which is expected to be miscible with a mesogenic compound. The selected LC molecule was MBBA, which is well known as a room temperature LC. The diffusion coefficients of pure MBBA obtained from the experiments and the MD simulation were found to be close each other, as described later. The **811** compound is miscible with MBBA, with a miscibility of at least 20 mol%. For each simulated system, the concentration of the dopant was set to ~0.1 mol%, and the number of molecules was listed in Table 1. The number of LC molecules were set to approximately 2000, as the system with this number of molecules can accurately reproduce the nematic-isotropic phase transition.

Table 1. Number of molecules in the five systems for pure MBBA, **N-Ru-Br0**, **N-Ru-Br1**, **N-Ru-trop**, and **N-811**.

System	LC Molecules	Chiral Dopant Molecule
Pure MBBA	2016	0
N-Ru-Br0	2004	2
N-Ru-Br1	2006	2
N-Ru-trop	2002	2
N-811	2003	2

The initial structure was constructed according to the methodology previously proposed [18]. In the initial structure of the pure MBBA, 2016 molecules were randomly placed without overlapping in a cubic periodic boundary box with an 11.4 nm side length. For the system in which Δ- and Λ-isomers were added to MBBA molecules, these isomers were placed not to interact with each other at the initial state.

The generalized Amber force field [19] parameters were used for the force field parameters for MBBA and chiral dopant molecules, while the universal force field (UFF) [20] parameters were applied to calculate the bond-stretching and bond-angle bending interactions, including interatomic bonds between ruthenium and its neighboring oxygen atoms. The partial atomic charges of the molecules were calculated using the restrained electrostatic potential (RESP) methodology [21] based on density functional theory (DFT) calculations (B3LYP/LANL2DZ for ruthenium atom and B3LYP/6-31G* for all other atoms) with the GAUSSIAN 09 revision E01 program.

The simulation procedure proposed in the previous study [18] involved pre-equilibration runs after the steepest energy minimization, which were performed as follows: 5 ns at 250 K and 1 bar, 1 ns at 350 K and 1 bar, and 5 ns at 300 K and 1 bar. During the pre-equilibration runs, the temperature and pressure were kept constant using a Berendsen thermostat and barostat [22] with relaxation times of 0.2 and 2.0 ps, respectively. The equilibration run was carried out for at least 300 ns at 300 K and 1 bar using a Nosé-Hoover thermostat [23–25] and Parrinello-Rahman barostat [26] with relaxation times of 1.0 and 5.0 ps, respectively. The time step was set to 2 fs, since all bonds connected to hydrogen atoms were constrained with the LINCS algorithm [27]. The long-range Coulomb interactions were calculated using the smooth particle-mesh Ewald method [28] with a grid spacing of 0.30 nm. The real space cutoff for both Coulomb and van der Waals interactions was 1.4 nm.

3. Results

Figure 2 shows the MD simulation snapshots of the simulated system, pure MBBA, **N-Ru-Br0**, **N-Ru-Br1**, **N-Ru-trop**, and **N-811**. In all the systems, Δ- and Λ-isomers were positioned away from each other, and no aggregations were formed. The MBBA molecules appeared to be aligned in one arbitrary direction in the snapshots, but the order parameter for the molecules must be calculated to understand the degree of molecular ordering.

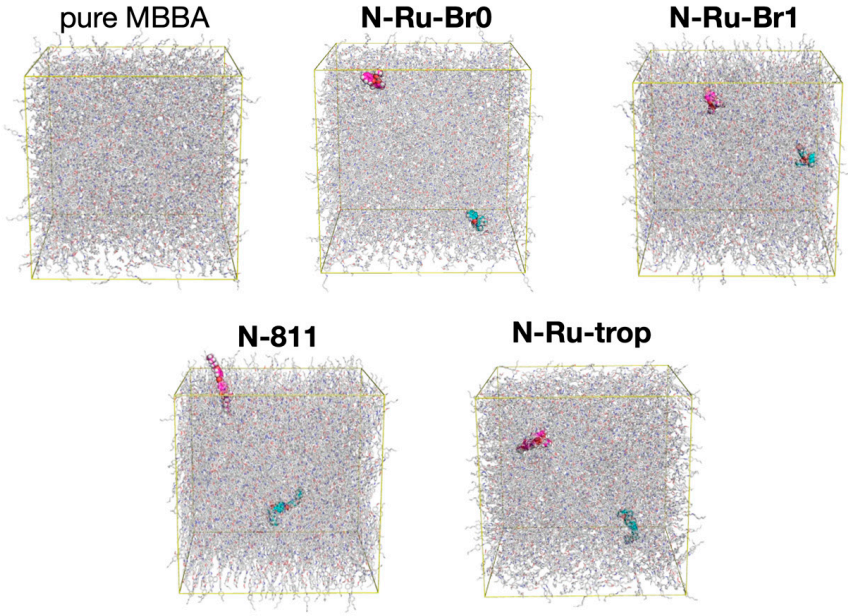

Figure 2. MD simulation snapshots of pure MBBA, **N-Ru-Br0**, **N-Ru-Br1**, **N-Ru-trop**, and **N-811** after the equilibration MD run. The carbon atoms of Δ- and Λ-isomers are colored in magenta and cyan, respectively. MBBA molecules are illustrated by sticks.

The order parameter S was estimated as the largest positive eigenvalue of the order parameter tensor $\boldsymbol{P}$, as expressed below:

$$P_{\alpha\beta} = \frac{1}{N}\sum_{i=1}^{N}\frac{1}{2}\left(3n_{i\alpha}n_{i\beta} - \delta_{\alpha\beta}\right) \quad (1)$$

where N is the total number of the LC molecules, subscripts α and β represent the coordinates x, y, and z, and $\boldsymbol{n}_i$ is the normalized long axis vector of the ith molecule. The long axis was defined as the vector connecting two end carbon atoms of the rigid aromatic core, as referred to in the previous study [29]. The time dependence of the nematic order parameter for the MBBA molecules was analyzed for each simulated system, as shown in Figure 3.

For the pure MBBA system, the order parameter averaged during the last 50 ns of the equilibration MD run was 0.57 ± 0.01 at 300 K. The system obtained from the MD simulations could exhibit the characteristics of bulk nematics, as the simulated order parameter is consistent with the experimental value for MBBA [30].

To confirm the validity of the simulation model and conditions, the temperature dependence of the order parameter for the pure MBBA system was also investigated, as shown in Figure 4. The order parameter at each temperature was the average of the last 50 ns of the equilibration MD run. Figure 4 indicates that the phase transition temperature for the MD simulation was close to the experimental value of 318 K.

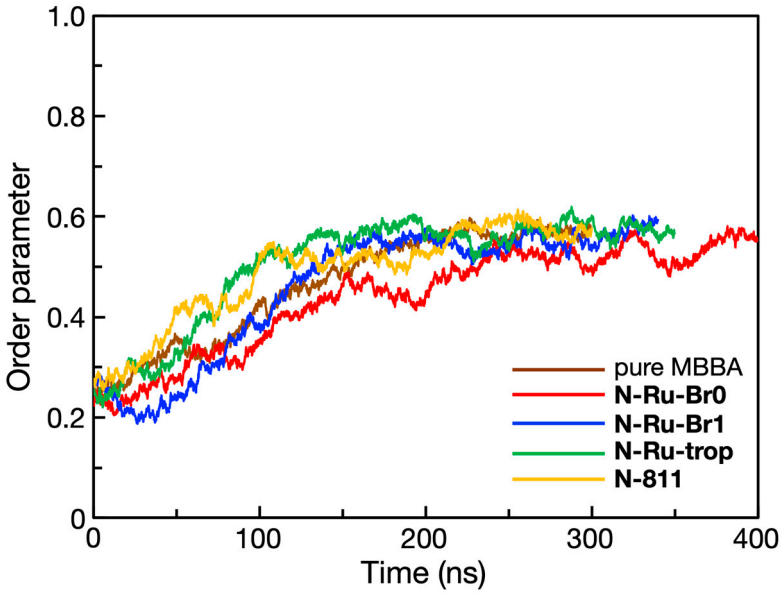

Figure 3. Time dependence of the nematic order parameter for pure MBBA, **N-Ru-Br0**, **N-Ru-Br1**, **N-Ru-trop**, and **N-811**. All the systems reached equilibration in the final 100 ns.

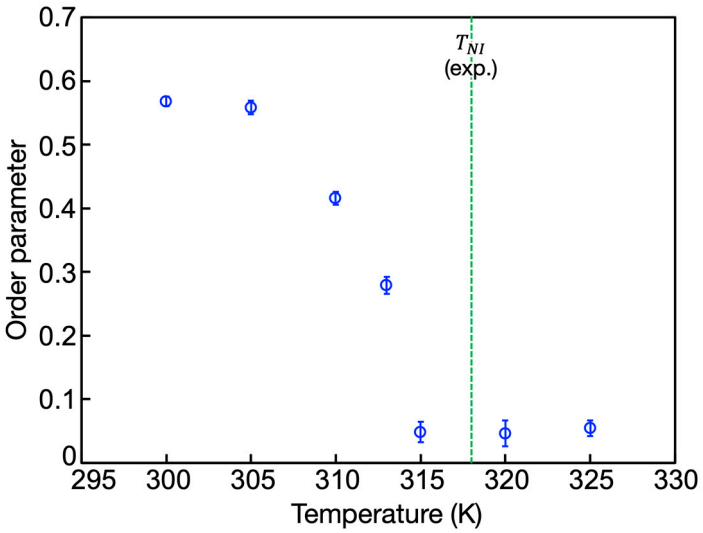

Figure 4. Temperature dependence of the nematic order parameter for pure MBBA. The values of the order parameter above 315 K were nearly zero, indicating that these systems were isotropic.

The order parameters averaged during the last 50 ns of the equilibration MD run were 0.57 ± 0.01, 0.54 ± 0.02, 0.57 ± 0.02, 0.58 ± 0.02, and 0.58 ± 0.02 for pure MBBA, **N-Ru-Br0**, **N-Ru-Br1**, **N-Ru-trop**, and **N-811**, respectively. These values indicate that these systems possessed the same degree of orientational order as that of the pure MBBA system.

The radial distribution functions are typically analyzed to investigate whether the simulated system has positional order. The radial distribution function (RDF) of the LC molecules, $g(r)$, is defined as:

$$g(r) = \frac{1}{4\pi r^2 \Delta r} \frac{V}{N} \frac{1}{N} \sum_{i=1}^{N} \Delta N_i(r) \quad (2)$$

where V is the total volume of the system, N is the total number of the LC molecules, $\Delta N_i(r)$ is the number of the LC molecules in the shell at a distance r from the ith molecule, and Δr is the thickness of the shell. As shown in Figure S1, the RDFs for all systems exhibit

similar curves, do not exhibit discrete sharp peaks, and asymptotically converge to 1. These characteristics of the RDFs are typical of those in the liquid state. It is shown that the LC molecules in the system were arranged in a disorderly manner without long-positional order. However, each of the RDFs had the first broad peak at approximately 0.5 nm, which is comparable to the length of the short axis of the MBBA molecule. This suggests a parallel arrangement with short-range order.

The diffusion properties of LC can be analyzed through all-atom MD simulation, providing important insights from a microscopic point of view [31]. The mean square displacements (MSDs) of the host MBBA molecules were analyzed, and the diffusion coefficients were calculated using Einstein's relation defined by following equation:

$$D = \frac{\langle |\boldsymbol{r}_i(t_0 + t) - \boldsymbol{r}_i(t_0)|^2 \rangle_i}{6t} = \frac{a}{6} \tag{3}$$

where $\boldsymbol{r}_i(t_0)$ is the molecular center-of-mass position at time t_0, and a is the slope of the linear fit of the MSD. Figure 5 indicates that the MBBA molecules in all the systems had significant fluidity. The diffusion coefficients of the MBBA molecules listed in Table 2 were of the same order of the magnitude as those reported in previous experiments [32]. Although the diffusion coefficients of the pure MBBA system, **N-Ru-trop**, and **N-811** were close to each other, the values were higher than those of **N-Ru-Br0** and **N-Ru-Br1**. Therefore, the more soluble the chiral dopant was in the nematics, the larger the diffusivity of the host LC molecules. This indicates that there is a correlation between the miscibility of the chiral dopant in the host LC solvent and the diffusion coefficient of the LC molecules.

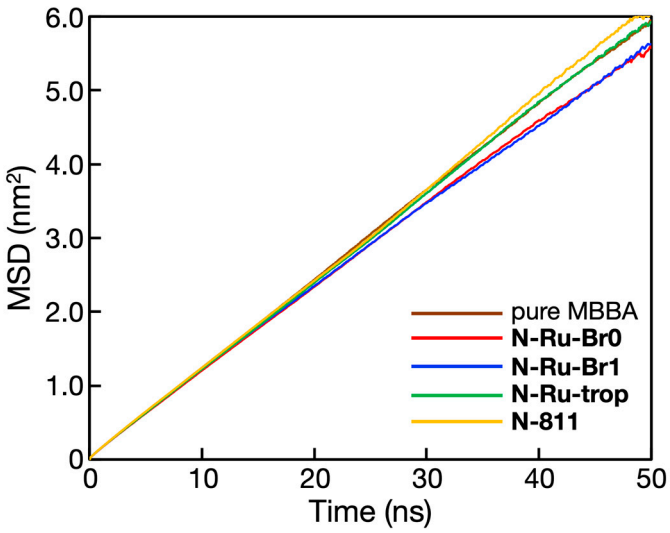

Figure 5. MSDs of MBBA molecules during the last 50 ns of equilibration runs for pure MBBA, **N-Ru-Br0**, **N-Ru-Br1, N-Ru-trop**, and **N-811**. The slope of the line was calculated using least square fitting between 15 ns and 45 ns.

Table 2. Diffusion coefficients (m^2/s) of MBBA in the five systems for pure MBBA, **N-Ru-Br0**, **N-Ru-Br1, N-Ru-trop**, and **N-811**.

	Pure MBBA	**N-Ru-Br0**	**N-Ru-Br1**	**N-Ru-trop**	**N-811**
D (m^2/s)	1.99 ± 0.01	1.87 ± 0.02	1.84 ± 0.02	2.00 ± 0.02	2.06 ± 0.04

Total interaction energy, which is defined as the sum of the van der Waal and Coulomb interaction energies, was calculated between the Δ-isomer of the chiral dopant molecule and the surrounding LC molecules for each system, and the time dependence is shown in Figure 6. There is little difference among the systems irrespective of the chiral ruthenium

complexes doped. The total interaction energies for pure MBBA and **N-811** were comparable and lower than those for the other three systems. No significant difference in the Coulomb interaction energy was seen among all the systems as shown in Figure S2. The van der Waals interaction energies of **Ru-Br0** and **Ru-Br1**, which are less miscible with LC, were larger than those of **Ru-trop** and **811** with high miscibility. This suggests that the van der Waals interaction energy between the chiral dopant and the host LC molecules affect its miscibility with the LC solvents.

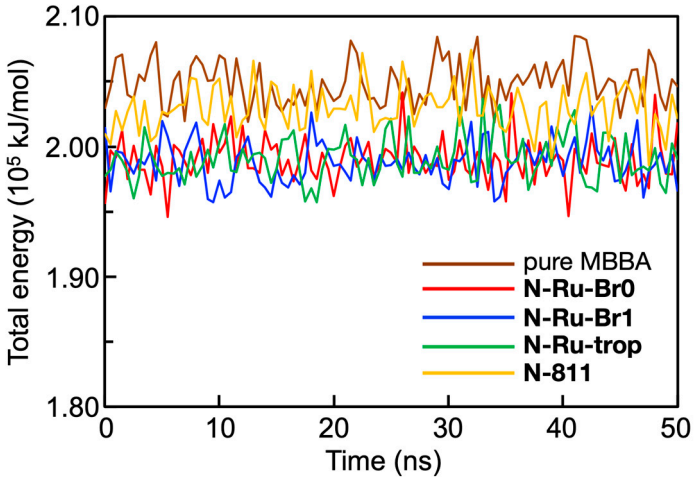

Figure 6. Time dependences of total interaction energies between the Δ-isomer of the chiral dopant molecule and the MBBA molecules for pure MBBA, **N-Ru-Br0**, **N-Ru-Br1, N-Ru-trop**, and **N-811** during the last 50 ns of the equilibration runs.

The MD simulations were performed for the systems with twice the concentration of **Ru-Br0** and **Ru-trop**. The time dependence of the order parameter of MBBA molecules for **N-Ru-Br0_2** with 0.2 mol% of **Ru-Br0** and **N-Ru-trop_2** with 0.2 mol% of **Ru-trop** is shown in Figure S4. The average order parameters of the LC molecules in the last 50 ns of the equilibration MD runs were 0.56 ± 0.01 and 0.59 ± 0.01, respectively. These values were similar to those of **N-Ru-Br0** and **N-Ru-trop**. From the slope of the MSD shown in Figure S7, the diffusion coefficients of MBBA molecules were estimated as $(1.74 \pm 0.01) \times 10^{-11}$ m^2/s and $(1.88 \pm 0.01) \times 10^{-11}$ m^2/s for **N-Ru-Br0_2** and **N-Ru-trop_2**, respectively. In both **N-Ru-Br0_2** and **N-Ru-trop_2**, compared to **N-Ru-Br0** and **N-Ru-trop** in which the concentrations of the chiral dopant were 0.1 mol%, the diffusion coefficients of the LC molecules were slightly smaller. Since the diffusion coefficient of the LC molecules of **N-Ru-trop_2** was significantly larger than that of **N-Ru-Br0_2**, the correlation between the diffusion property of the LC solvent and the miscibility of the chiral dopant was independent of its concentration. Figure S3 shows the time dependence of the total interaction energies, the van der Waals interaction energies, and Coulomb interaction energies between the Δ-isomer of the chiral dopant molecule and the LC molecules. There were no significant differences in the interaction energies depending on the concentration of chiral dopants.

In the initial structure of the systems described above, the chiral dopant molecules were dispersed into the LC molecules and did not form any aggregates during the equilibration runs. It is crucial to determine whether the dopants are dispersed in nematic liquid crystals. To confirm the dispersibility of the dopants in detail, MD simulations were performed for the systems in which a pair of Δ- and Λ-isomers was placed in the LC solvent as an aggregated initial structure. The simulated systems are denoted as **N-Ru-Br0_agg** and **N-Ru-trop_agg**, containing MBBA molecules and **Ru-Br0** and **Ru-trop**, respectively. During the pre-equilibrium and the following equilibration runs, a pair of Δ- and Λ-isomers was restrained in the initial position by applying the harmonic potential with a force constant of 1000 $kJ/mol/nm^2$. After 200 ns, during which the system reached the equilibrated state

(Figure S4), an equilibration run without any restraints was performed for 400 ns (Figure S6). In both **N-Ru-Br0_agg** and **N-Ru-trop_agg**, the aggregation was not stable, and the two isomers individually diffused in the nematic solvent (Figure 7). The distance between the isomers was approximately 4.0 nm, as shown in Figure S9. The MSDs of MBBA molecules for the last 50 ns of the equilibration run with no restraints were analyzed, as shown in Figure S8, and the diffusion coefficients were estimated as $(1.84 \pm 0.02) \times 10^{-11}$ m^2/s and $(1.95 \pm 0.01) \times 10^{-11}$ m^2/s for **N-Ru-Br0_agg** and **N-Ru-trop_agg**, respectively. The LC molecules in **N-Ru-trop_agg** diffused slightly faster than those in **N-Ru-Br0_agg**. The value of the diffusion coefficient of the LC molecules in **N-Ru-trop_agg** was nearly the same as those in pure MBBA and **N-Ru-trop.** This indicates that the systems in which the aggregate of Δ- and Λ-isomers was initially placed in the LC solvents exhibited the same behavior as those in which the isomers were initially separated. Since the difference in the formation of the chiral molecules in the initial structure had little effect on the physical properties, the validity of the initial structures of **N-Ru-Br0**, **N-Ru-Br1**, **N-Ru-trop**, and **N-811** was also confirmed.

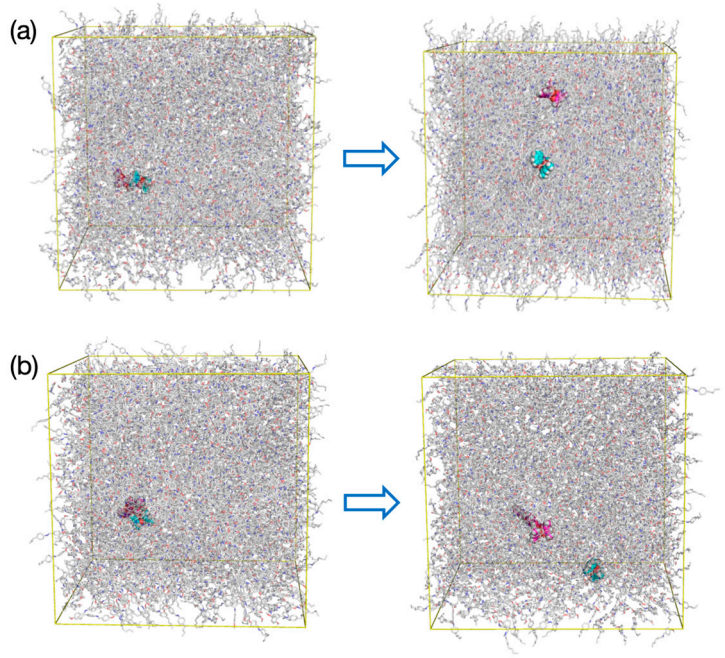

Figure 7. MD simulation snapshots of (**a**) **N-Ru-Br0_agg** and (**b**) **N-Ru-trop_agg** at 0 ns (**left**) and at 400 ns (**right**) of the equilibration run without any restraints. The carbon atoms of Δ- and Λ-isomers are colored in magenta and cyan, respectively. MBBA molecules are illustrated by sticks.

4. Summary

In this study, all-atom MD simulations for the racemic systems in which both the Δ- and Λ-enantiomers of the chiral dopant molecule were doped into the nematic LC molecul, for **Ru-Br0**, **Ru-Br1**, **Ru-trop**, and **811**. By investigating the microscopic behavior of the chiral dopant and LC molecules, we aimed to understand the factor that causes the difference in the miscibility of the chiral dopant analogues in the nematic solvents.

The nematic order parameters of LC molecules for all the systems into which the chiral dopant molecules were doped were the same as that of the pure LC system. At low concentrations of the chiral dopants, such as 0.1 mol%, they had little effect on the orientational order of the surrounding LC molecules.

By analyzing the MSDs and diffusion coefficients of the LC molecules, the miscibility of the chiral dopant in the host LC solvent and the diffusion behavior of the LC molecules were found to be correlated. In the system to which the chiral dopant molecules with high miscibility were added, the diffusion coefficient of the LC solvents was comparable to that

of the system without the chiral molecule. This indicates that the diffusion property, i.e., the viscosity of the LC molecules, was less affected by the chiral dopant molecule with higher miscibility.

The analysis of the interaction energies between the chiral dopant molecule and LC molecules showed that the van der Waals interaction energies were correlated with the miscibility of the dopant molecule. The molecular shapes of **Ru-trop** and **811**, which are highly miscible with MBBA solvent, are more elongated compared to **Ru-Br0** and **Ru-Br1**. The aspect ratio of the molecular length parallel to the C_2 axis to that perpendicular to the C_2 axis for each ruthenium complex molecule was approximately 1.6, 1.5, and 4.0 for **Ru-Br0**, **Ru-Br1**, and **Ru-trop**, respectively. These molecules are derivatives with the same rigid octahedral ruthenium core, but the shape of **Ru-trop** is more rod-like and anisotropic compared to that of **Ru-Br0** and **Ru-Br1**. This indicates that more elongated chiral dopants were more miscible with the nematic solvent consisting of calamitic molecules, and that those dopant molecules had little influence on the diffusion behavior of the nematic LC molecules.

Moreover, it is of interest to investigate how the sign of dielectric anisotropy and the abundance of the ion in the LC molecules influence on their diffusion behaviors. To address these issues, we plan to conduct additional MD simulations using different solvents in the future.

Several theoretical and computational methods to have been developed to accurately calculate the thermodynamic and structural properties of solvation [33]. However, predicting the miscibility of organic molecules in anisotropic fluids remains challenging, even though solvation free energies for small gas molecules have been calculated by determining the free energy change for transferring each gas molecule from an ideal gas vapor phase to bulk LC [34].

Performing MD simulations using the model and procedure presented in this paper may enable us to predict the miscibility of a newly designed dopant molecule in nematic LC solvents before synthesizing the dopant. This approach could help facilitate the development of novel chemical compounds more efficiently than ever before.

Supplementary Materials: The following supporting information can be downloaded at https://www.mdpi.com/article/10.3390/sym15051092/s1.

Author Contributions: A.Y. and G.W. performed MD simulations and analysis. J.Y. and G.W. co-wrote manuscript. All authors have read and agreed to the published version of the manuscript.

Funding: The computations were partially performed at the Research Center for Computational Science, Okazaki, Japan (Project: 21-IMS-C043, 22-IMS-C043). This work was supported by the Grant-in-Aid for Scientific Research (B) (JP19H02537), Grant-in-Aid for Scientific Research (C) (JP19K05508), Grant-in-Aid for Scientific Research on Innovative Areas (JP19H05718), and Grant-in-Aid for Challenging Research (Exploratory) (JP22K18953).

Data Availability Statement: The data presented in this study are available on request from the corresponding author (G.W.).

Conflicts of Interest: The authors declare no conflict of interest.

References

1. Solladié, G.; Zimmermann, R.G. Liquid Crystals: A Tool for Studies on Chirality. *Angew. Chem. Int. Ed.* **1984**, *23*, 348–362. [CrossRef]
2. de Gennes, P.G.; Prost, J. *The Physics of Liquid Crystals*, 2nd ed.; Oxford University Press: Oxford, UK, 1993.
3. Kitzerow, H.-S.; Bahr, C. (Eds.) *Chirality in Liquid Crystals*; Springer: New York, NY, USA, 2001.
4. Goodby, J.W.; Collings, P.J.; Kato, T.; Tschierske, C.; Gleeson, H.; Raynes, P. (Eds.) *Handbook of Liquid Crystals*; Wiley-VCH Verlag GmbH & Co. KGaA: Weinheim, Germany, 2014.
5. Finkelmann, H.; Kim, S.T.; Muñoz, A.; Palffy-Muhoray, P.; Taheri, B. Tunable mirrorless lasing in cholesteric liquid crystalline elastomers. *Adv. Mater.* **2001**, *13*, 1069–1072. [CrossRef]
6. Matsui, T.; Ozaki, R.; Funamoto, K.; Ozaki, M.; Yoshino, K. Flexible mirrorless laser based on a free-standing film of photopolymerized cholesteric liquid crystal. *Appl. Phys. Lett.* **2002**, *81*, 3741–3743. [CrossRef]

7. Araoka, F.; Shin, K.C.; Takanishi, Y.; Ishikawa, K.; Takezoe, H.; Zhu, Z.; Swager, T.M. How doping a cholesteric liquid crystal with polymeric dye improves an order parameter and makes possible low threshold lasing. *J. Appl. Phys.* **2003**, *94*, 279–283. [CrossRef]
8. Yang, D.K.; Doane, J.W.; Yaniv, Z.; Glasser, J. Cholesteric Reflective Display: Drive Scheme and Contrast. *Appl. Phys. Lett.* **1994**, *64*, 1905–1907. [CrossRef]
9. Tamaoki, N. Cholesteric Liquid Crystals for Color Information Technology. *Adv. Mater.* **2001**, *13*, 1135–1147. [CrossRef]
10. Hsiao, Y.-C.; Yeh, E.-R.; Lee, W. Advanced Color-Reflective Dual-Frequency Cholesteric Liquid Crystal Displays and the Driving Matrix. *Mol. Cryst. Liq. Cryst.* **2017**, *644*, 12–18. [CrossRef]
11. Yu, B.H.; Huh, J.W.; Heo, J.; Yoon, T.H. Simultaneous Control of Haze and Transmittance Using a Dye-Doped Cholesteric Liquid Crystal Cell. *Liq. Cryst.* **2015**, *42*, 1460–1464. [CrossRef]
12. Oh, S.-W.; Kim, S.-H.; Baek, J.-M.; Yoon, T.-H. Optical and Thermal Switching of Liquid Crystals for Self-Shading Windows. *Adv. Sustain. Syst.* **2018**, *2*, 1700164. [CrossRef]
13. Li, C.; Tseng, H.; Chen, C.; Wang, C.; Jau, H.; Wu, Y.; Hsu, W.; Lin, T.H. Versatile Energy-Saving Smart Glass Based on Tristable Cholesteric Liquid Crystals. *ACS Appl. Energy Mater.* **2020**, *3*, 7601–7609. [CrossRef]
14. Han, Y.; Pacheco, K.; Bastiaansen, C.W.M.; Broer, D.J.; Sijbesma, R.P. Optical Monitoring of Gases with Cholesteric Liquid Crystals. *J. Am. Chem. Soc.* **2010**, *132*, 2961–2967. [CrossRef] [PubMed]
15. Zhang, W.; Schenning, A.P.H.J.; Kragt, A.J.J.; Zhou, G.; de Haan, L.T. Thermochromic Multicolored Photonic Coatings with Light Polarization- and Structural Color-Dependent Changes. *ACS Appl. Polym. Mater.* **2022**, *4*, 537–545. [CrossRef]
16. Yoshida, J.; Tamura, S.; Watanabe, G.; Kasahara, Y.; Yuge, H. "Colored" Inorganic Dopants for Inducing Liquid Crystal Chiral Nematic and Blue Phases: Monitoring of Dopant-Host Interaction by Raman Spectroscopy. *Chem. Commun.* **2017**, *53*, 5103–5106. [CrossRef]
17. Yoshida, J.; Tamura, S.; Hoshino, K.; Yuge, H.; Sato, H.; Yamazaki, A.; Yoneda, S.; Watanabe, G. Comprehensive Understanding of Host- and Guest-Dependent Helix Inversion in Chiral Nematic Liquid Crystals: Experimental and Molecular Dynamics Simulation Study. *J. Phys. Chem. B* **2018**, *122*, 10615–10626. [CrossRef]
18. Yoshida, J.; Watanabe, G. Molecular Dynamics Approach for Predicting Helical Twisting Powers of Metal Complex Dopants in Nematic Solvents. *J. Phys. Chem. B* **2016**, *120*, 6858–6864.
19. Wang, J.; Wolf, R.M.; Caldwell, J.W.; Kollman, P.A.; Case, D.A. Development and Testing of a General Amber Force Field. *J. Comput. Chem.* **2004**, *25*, 1157–1174. [CrossRef] [PubMed]
20. Rappe, A.K.; Casewit, C.J.; Colwell, K.S.; Goddard III, W.A.; Skiff, W.M. UFF, a Full Periodic Table Force Field for Molecular Mechanics and Molecular Dynamics Simulations. *J. Am. Chem. Soc.* **1992**, *114*, 10024–10035. [CrossRef]
21. Bayly, C.I.; Cieplak, P.; Cornell, W.; Kollman, P.A. A Well-Behaved Electrostatic Potential Based Method Using Charge Restraints for Deriving Atomic Charges: The RESP Model. *J. Phys. Chem.* **1993**, *97*, 10269–10280. [CrossRef]
22. Berendsen, H.J.C.; Postma, J.P.M.; van Gunsteren, W.F.; DiNola, A.; Haak, J.R. Molecular Dynamics with Coupling to an External Bath. *J. Chem. Phys.* **1984**, *81*, 3684–3690. [CrossRef]
23. Nosé, S. A Molecular Dynamics Method for Simulations in the Canonical Ensemble. *Mol. Phys.* **1984**, *52*, 255–268. [CrossRef]
24. Nosé, S. A unified formulation of the constant temperature molecular dynamics methods. *J. Chem. Phys.* **1984**, *81*, 511–519. [CrossRef]
25. Hoover, W.G. Canonical dynamics: Equilibrium phase-space distributions. *Phys. Rev. A* **1985**, *31*, 1695–1697. [CrossRef] [PubMed]
26. Parrinello, M.; Rahman, A. Polymorphic Transitions in Single Crystals: A New Molecular Dynamics Method. *J. Appl. Phys.* **1981**, *52*, 7182–7190. [CrossRef]
27. Hess, B.; Bekker, H.; Berendsen, H.J.C.; Fraaije, J.G.E.M. LINCS: A linear constraint solver for molecular simulations. *J. Comput. Chem.* **1997**, *18*, 1463–1472. [CrossRef]
28. Essmann, U.; Perera, L.; Berkowitz, M.L.; Darden, T.; Lee, H.; Pedersen, L.G. A smooth particle mesh Ewald method. *J. Chem. Phys.* **1995**, *103*, 8577–8593. [CrossRef]
29. Watanabe, G.; Saito, J.; Kato, N.; Tabe, Y. Orientational correlations in two-dimensional liquid crystals studied by molecular dynamics simulation. *J. Chem. Phys.* **2011**, *134*, 054513. [CrossRef]
30. Subramhanyam, H.S.; Prabha, C.S.; Krishnamurti, D. Optical Anisotropy of Nematic Compounds. *Mol. Cryst. Liq. Cryst.* **1974**, *28*, 201–215. [CrossRef]
31. Watanabe, G.; Saito, J.; Fujita, Y.; Tabe, Y. Molecular Dynamics Simulation Study of Two-Dimensional Diffusion Behavior in Smectic Liquid Crystalline Monolayers. *J. Phys. Soc. Jpn.* **2013**, *82*, 084603. [CrossRef]
32. Ohta, K.; Terazima, M.; Hirota, N. Diffusion Process of a Liquid Crystal Probed by the Transient Grating Method. *Bull. Chem. Soc. Jpn.* **1995**, *68*, 2809–2815. [CrossRef]
33. Ratkova, E.L.; Palmer, D.S.; Fedorov, M.V. Solvation Thermodynamics of Organic Molecules by the Molecular Integral Equation Theory: Approaching Chemical Accuracy. *Chem. Rev.* **2015**, *115*, 6312–6356. [CrossRef]
34. Sheavly, J.K.; Gold, J.I.; Mavrikakis, M.; Van Lehn, R.C. Molecular simulations of analyte partitioning and diffusion in liquid crystal sensors. *Mol. Syst. Des. Eng.* **2020**, *5*, 304–316. [CrossRef]